Visualizing Second-Order Tensor Fields with Hyperstreamlines

Article *in* IEEE Computer Graphics and Applications · August 1993

DOI: 10.1109/38.219447 · Source: IEEE Xplore

2 authors, including:

Lambertus Hesselink
Stanford University
439 PUBLICATIONS **10,849** CITATIONS

SEE PROFILE

Visualizing Second-Order Tensor Fields with Hyperstreamlines

Thierry Delmarcelle and Lambertus Hesselink
Stanford University

We can use hyperstreamlines—a generalization of vector field streamlines—to visualize 3D second-order tensor fields along continuous paths.

Because scientists don't have proper tensor-display techniques, they now visualize many physical problems incompletely in terms of vector or scalar data. Scientists could undoubtedly get new insights into these problems if they had a methodology for visualizing 3D second-order tensor fields. We present *hyperstreamlines* as a way of visualizing these data.

Second-order tensor fields are fundamental in engineering and the physical sciences. Stresses and strains in solids, for example, are tensor fields. In fluid flows, stresses, viscous stresses, rate of strain, and momentum transfers are all described in terms of tensor data. In fact, the steady-state Navier-Stokes equations describe gas flows with only one quantity—momentum flux density—which is itself a tensor field.

Table 1 lists for reference some common tensor fields that we analyze in more detail later. It shows that tensor data carry a large amount of information. They include diverse physical quantities such as pressure, kinetic energy density, mass density, velocity, and derivatives of the velocity field. Visualizing tensor fields correlates these quantities. (More information about tensor fields can be found in Borisenko and Tarapov's book.[1])

Because of the wealth of multivariate information in tensor fields, tensor visualization is a challenge. Indeed, a 3D second-order tensor field $\mathbf{T}$ consists of a 3×3 array of scalar functions $\{T_{ik}\}$, $i, k = 1, 2, 3$ defined over a 3D domain. Independent visualization of these nine functions is possible but meaningless.

To help scientists visualize 3D tensor data, we have developed a methodology based on the concept of a hyperstreamline, the simplest continuous tensor structure that can be extracted from a tensor field (as opposed to many other scalar or vector features). We first introduce hyperstreamlines for the particular case of symmetric tensor fields $\mathbf{U} = \{U_{ik}\}$, whose individual components are related to each other by $U_{ik} = U_{ki}$ for $i, k = 1, 2, 3$. (As seen in Table 1, symmetric tensor fields are very common in fluid-flow studies.) We later derive a structural depiction of symmetric tensor fields from the representation of many hyperstreamlines. And, finally, we provide a methodology to visualize unsymmetric tensor data by encoding an additional vector field along the trajectory of the hyperstreamlines.

Symmetric tensor fields and hyperstreamlines

Symmetric tensor fields $\mathbf{U} = \{U_{ik}\} = \{U_{ki}\}$ are common in physics and engineering, so visualizing them is an important challenge. Visualizing symmetric tensor fields is also necessary for displaying general unsymmetric data, which we will address later.

We can describe a symmetric tensor $\mathbf{U}$ by three orthogonal vector fields. Indeed, $\mathbf{U}$ has at every point x three real eigenvalues $\lambda^{(i)}$, $i = 1, 2$, or 3 ordered according to

$$\lambda^{(1)} \geq \lambda^{(2)} \geq \lambda^{(3)}$$

0272-17-16/93/0700-0025$03.00 © 1993 IEEE

Table 1. Tensor fields in fluid flows.

$v_{i,k} = \frac{\partial v_i}{\partial x_k}^*$	Velocity gradient (u)
$\varepsilon_{ik} = v_{i,k} + v_{k,i}$	Rate-of-strain tensor (s)
$\sigma'_{ik} = \eta\varepsilon_{ik}$ **	Viscous-stress tensor (s)
$\sigma_{ik} = -p\delta_{ik} + \sigma'_{ik}$	Stress tensor (s)
$\Pi^r_{ik} = p\delta_{ik} + \rho v_i v_k$	Reversible momentum flux density tensor (s)
$\Pi_{ik} = \Pi^r_{ik} - \sigma'_{ik}$	Momentum flux density tensor (s)

* In non-Cartesian coordinate systems, covariant derivatives must be used instead.
** In compressible flows, there is an additional term involving the divergence of the velocity field.
p = pressure
ρ = mass density
v_i and v_k = velocity components
η = viscosity
δ_{ik} = Kronecker symbol
(u) = unsymmetric
(s) = symmetric

as well as three real and orthogonal unit eigenvectors $\bar{e}^{(i)}$.[1] We consider the three orthogonal vectors $\bar{v}^{(i)}$ given by

$$\bar{v}^{(i)} = \lambda^{(i)}\ \bar{e}^{(i)} \qquad \textbf{(1)}$$

Because of the ordering of the eigenvalues, we refer to $\bar{v}^{(1)}$ as the *major eigenvector,* $\bar{v}^{(2)}$ as the *medium eigenvector,* and $\bar{v}^{(3)}$ as the *minor eigenvector.*

Visualizing **U** is fully equivalent to visualizing simultaneously the three vector fields $\bar{v}^{(i)}$, since they include all the amplitude information (the eigenvalues $\lambda^{(i)}$) and all the directional information (the unit eigenvectors $\bar{e}^{(i)}$) represented in matrix notation by the components U_{ik}. Furthermore, as we stated in our earlier work,[2] visualizing the three vectors $\bar{v}^{(i)}$ can help users with little or no training understand the behavior of the six independent components U_{ik}.

In previously developed methods, researchers visualized these three vectors at some coarsely spaced points by using point tensor icons. Examples of such icons include Haber's tensor glyphs or ellipsoids having the three vectors $\bar{v}^{(i)}$ for principal axes.[3,4] Point icons represent all the tensor information at a given location, but their discrete nature does not reveal the underlying continuity of the data field. For this reason, Dickinson[5] used *tensor-field lines*, streamlines of one of the eigenvector fields $\bar{v}^{(i)}$. While emphasizing data continuity, tensor-field lines are only vector icons and represent the tensor field only partially. (This is analogous to representing a vector field by examining only one of its scalar components.)

Instead of only partially representing the tensor field, we want a line tensor icon that represents all the tensor information along a 3D path in space or, equivalently, an icon that encodes a continuous distribution of ellipsoids along a given trajectory. For this purpose, we generalize the vector notion of a streamline to the tensor concept of a hyperstreamline:

> A geometric primitive of finite size sweeps along one of the eigenvector fields $\bar{v}^{(i)}$ while stretching in the transverse plane under the combined action of the two other orthogonal eigenvector fields. A hyperstreamline is the surface obtained by linking the stretched primitives at the different points along the trajectory. It is color-coded by means of a user-defined function of the three eigenvalues, generally the amplitude of the longitudinal eigenvalue.

The color and trajectory of a hyperstreamline fully represent the longitudinal eigenvector field, and the cross section encodes the two remaining transverse eigenvector fields. Thus, hyperstreamlines form a continuous representation of all the tensor data along the trajectory. Hyperstreamlines are called major, medium, or minor depending on the longitudinal eigenvector field $\bar{v}^{(i)}$ that defines the trajectory. In Figures 1 and 2, we illustrate the properties of hyperstreamlines for two elastic stress fields in a semi-infinite steel solid. We describe these in detail below.

Trajectory of a hyperstreamline

Hyperstreamline trajectories correspond to Dickinson's tensor-field lines.[5] These patterns of lines show, for example, how forces propagate in a stress-tensor field and how the momentum is transferred in a momentum flux density tensor field. Figure 1a illustrates this phenomenon in an elastic stress-tensor field induced by two compressive forces onto the top surface of the material.

We color-coded every line according to the longitudinal eigenvalue. The lines propagating upward are along the most compressive direction (the minor eigenvector $\bar{v}^{(3)}$). They converge toward the regions of high stress, where the forces are applied. Note the sudden divergence of close trajectories on each side of the plane of symmetry. Similarly, trajectories along the two other eigenvectors delineate a surface shown near the bottom face of the cube. This surface is everywhere perpendicular to the most compressive direction.

Cross section of a hyperstreamline

Hyperstreamlines are further characterized by the geometry of their cross section, that is, the geometric primitive that sweeps along the trajectory. We consider two types of primitives:

1. A circle that stretches into an ellipse while sweeping and that generates a hyperstreamline called a *tube.*
2. A cross that generates a hyperstreamline called a *helix.*

Figure 1b shows two minor tubes propagating upward and four medium and major helices in the stress-tensor field corre-

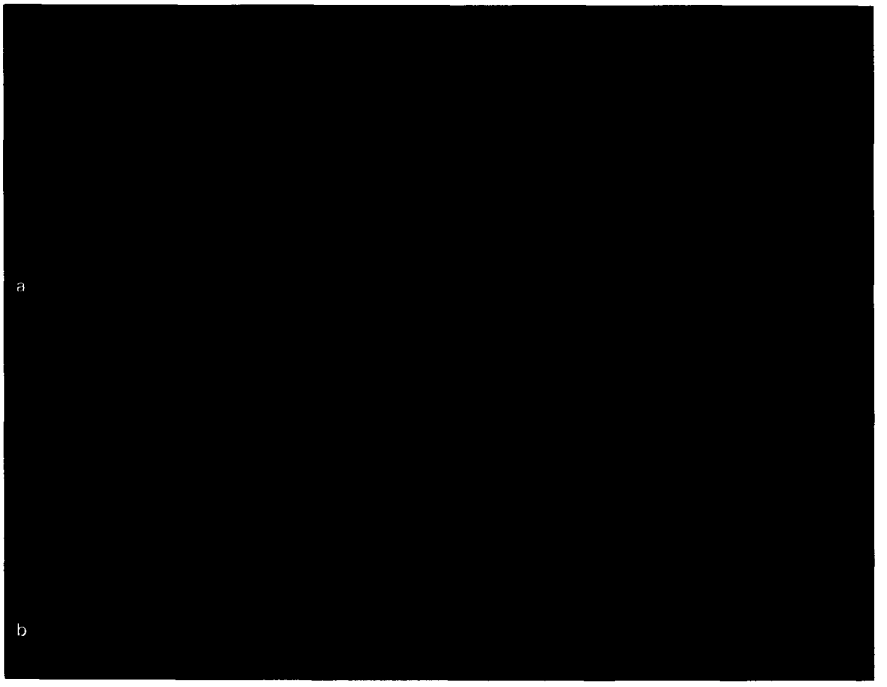

Figure 1. A stress tensor induced by two compressive forces. (a) Hyperstreamline trajectories; (b) minor tubes and medium and major helices; and (c) solenoidal property of a minor tube. We used Color Scale A from Figure 2.

sponding to Figure 1a. In a tube, the principal axes of each elliptical cross section are along the transverse eigenvectors and have a length proportional to the magnitude of the transverse eigenvalues. The same property holds for a helix, whose arms are proportional to the transverse eigenvectors. (Helices owe their name to the spiraling pattern of their arms, which you can see in some cases.) In this manner, we encode both directional and amplitude information along the trajectory. We can detect the local sign of the transverse eigenvalues by examining the singularities in the hyperstreamline's cross section. Indeed, the cross section reduces to one line or a point wherever one of the transverse eigenvalues changes sign.

Tubes and helices encode the same information about the tensor field, but viewers can see some aspects of the data better with one hyperstreamline than the other. Tubes, for instance, better show where the tensor is degenerate in the transverse plane, since recognizing that an ellipse is circular is easier than comparing the length of two perpendicular line segments. Further, if the tensor field is transversely degenerate in a whole region of space, helices are not adequate, because the direction of the transverse eigenvectors is not determined. On the other hand, helices more precisely show the directions of the transverse eigenvectors.

In Figure 2, we display four different stages of a minor tube in a stress-tensor field. The tensor field is similar to that of Figure 1, but we added another tension force. In Figure 2a, the cross section is circular, and the transverse stresses are equal in magnitude. Figure 2b shows an increasing anisotropy of the transverse stresses together with a decrease of the longitudinal eigenvalue (color). In Figure 2c, the cross section is reduced to a straight line; one

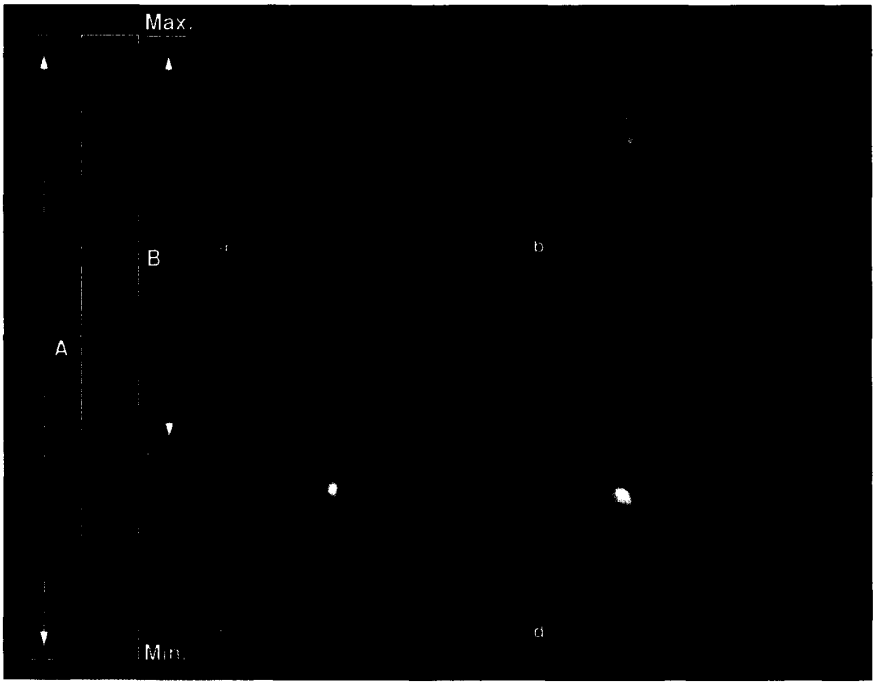

Figure 2. Four different stages of a minor tube in an elastic stress-tensor field. We used Color Scale A.

Figure 3. Rake of major tubes of the momentum flux density tensor in the flow past an ogive cylinder. Again we used Color Scale A as shown in Figure 2.

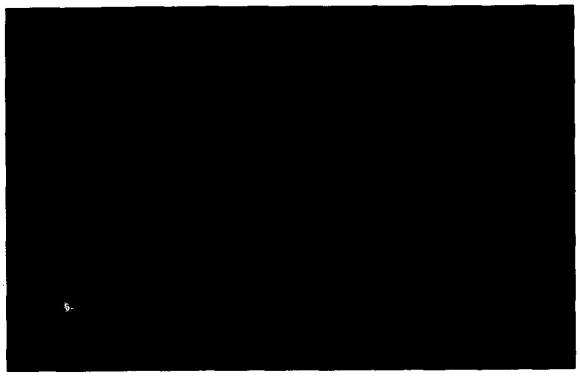

transverse eigenvalue is zero and the stresses are locally 2D. In Figure 2d, the stresses are 3D once again. The eigenvectors undergo a rapid rotation and a substantial stretching that reveals an important gradient of shear and pressure in the region.

Degenerate and singular points

Computing hyperstreamlines is complicated because degeneracies—points where two eigenvalues become equal to each other—can occur along the trajectory at and in between the sampling points requested by the adaptive integration algorithm. We assume that the tensor field is smooth. That is, we assume that the direction of the longitudinal eigenvector is not likely to vary by more than a user-predefined angle between two successive sampling points. But if the direction of the longitudinal eigenvector changes abruptly, we suspect that the trajectory just crossed a degeneracy involving the longitudinal eigenvalue. Then, we search for the degeneracy between the last two sampling points and, if found, terminate the curve there. We can then jump the degeneracy and continue integrating in a selected eigendirection. We also detect the points where the transverse eigenvalues vanish and include these points in the curve so that we don't miss a singularity of the cross section of the hyperstreamline.

Solenoidal tensor fields

In general, the hyperstreamlines' color varies along the trajectory. In some tensor fields, this variation in color captures some behavior of neighboring hyperstreamlines. We define these tensor fields as *solenoidal* by analogy with the properties of solenoidal vector fields.

A vector field $\vec{v}$ is solenoidal if it is divergence-free, that is

$$\sum_{i=1}^{3} \frac{\partial v_i}{\partial x_i} = 0$$

Examples of solenoidal vector fields include the vorticity or the velocity in incompressible flows. We can explain much of the structure of solenoidal vector fields by their property of having a constant flux inside a stream tube.[1] The magnitude of the vector field must increase locally in regions where the streamlines converge and decrease where the streamlines diverge.

By analogy, a tensor field $\mathbf{U}$ is solenoidal if it satisfies

$$\sum_{i=1}^{3} \frac{\partial \mathbf{U}_{ik}}{\partial x_i} = 0 \qquad \textbf{(2)}$$

for $k = 1, 2, 3$. This implies that the three vector fields obtained by multiplying $\mathbf{U}$ by any three constant orthogonal directions are solenoidal.

Solenoidal tensor fields are not rare mathematical objects. They are fundamental to fluid and solid-state mechanics. For example, the stress tensor σ_{ik} in solids at rest (in regions where no external forces are applied) and the momentum flux density tensor Π_{ik} in gravity-free, steady-state fluid flows both satisfy Equation 2, and both are solenoidal tensor fields. (The assumption of no gravity is common when computing gas flows.) However, the stress and viscous-stress tensors in fluid flows are not solenoidal.

Hyperstreamlines of solenoidal tensor fields have a "convergence and divergence" property analogous to the property of streamlines in solenoidal vector fields. More precisely, if $\lambda^{(i)}$ is the longitudinal eigenvalue of a hyperstreamline along the eigenvector $\vec{v}^{(i)}$, and if $\lambda^{(j)}$ and $\lambda^{(k)}$ are the two transverse eigenvalues, then Equation 2 is equivalent to

$$\lambda^{(i)\prime} = K_{ij}(\lambda^{(i)} - \lambda^{(j)}) + K_{ik}(\lambda^{(i)} - \lambda^{(k)}) \qquad \textbf{(3)}$$

where $\lambda^{(i)\prime}$ is the derivative of the longitudinal eigenvalue along the trajectory. K_{ij} and K_{ik} are geometric factors that are positive if neighboring hyperstreamlines along $\vec{v}^{(i)}$ converge in the corresponding transverse directions j or k. These factors (K_{ij} and K_{ik}) are negative otherwise. Thus, when the longitudinal eigenvalue of a major hyperstreamline increases during its propagation ($\lambda^{(i)\prime} > 0$), neighboring major hyperstreamlines converge. Any divergence in one transverse eigendirection must be compensated by a stronger convergence in the other transverse eigendirection. The opposite property holds true for minor hyperstreamlines: an increasing longitudinal (minor) eigenvalue correlates with a global divergence of neighboring minor hyperstreamlines. If they converge in one transverse eigendirection, they must diverge more strongly in the other. Conversely, a decreasing longitudinal eigenvalue corresponds to diverging major hyperstreamlines and converging minor hyperstreamlines.

It follows, then, that encoding the longitudinal eigenvalue into the color of a hyperstreamline in a solenoidal tensor field gives information about the behavior of neighboring hyperstreamlines. The figure at the beginning of this article illustrates this property for major tubes of the momentum flux density tensor in the flow past a hemisphere cylinder. Longitudinal eigenvalue (color) decreases as the trajectories diverge.

Equation 3 also explains why the minor hyperstreamlines in Figure 1 converge toward the applied forces (quickly decreasing longitudinal eigenvalue) and why the major hyperstreamlines propagate mostly parallel to each other with an almost constant color. In Figure 1c, we give a close view of the sudden divergence of minor hyperstreamlines on one side of the plane of symmetry. The local divergence of minor trajectories creates a sudden increase of the longitudinal eigenvalue (color). This contradicts the notion that the minor (most compressive)

Figure 4. Reversible momentum flux density tensor in the flow past a hemisphere cylinder. Again we used Color Scale A as shown earlier.

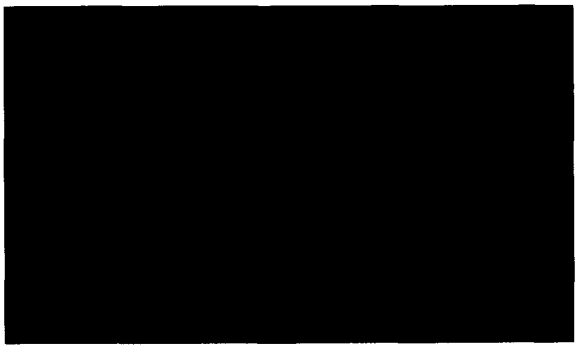

eigenvalue should decrease uniformly when approaching one of the two applied compressive forces.

In Figure 3, we show a rake of major tubes of the momentum flux density tensor, Π_{ik} (see Table 1), in the flow past an ogive cylinder. The air flow comes in from a direction five degrees to the left of the ogive axis, and vortices are created in the wake of the body. Major tubes that become entangled in the vortices undergo a fast decrease in color while diverging from each other. In other regions of the flow, the color remains constant. In some places, it even increases slightly from orange to red. In these regions, the apparent divergence of the tubes in the direction parallel to the surface of the body is compensated by a stronger convergence in the perpendicular direction. Both divergence and convergence exactly compensate each other in the tail between the two vortices.

Reversible momentum flux density tensor

With a specific example of fluid flow analysis, let's look at how we might use hyperstreamlines to correlate several different physical quantities. For the reversible part of the momentum flux density tensor, Π^r_{ik} (see Table 1), we might correlate pressure p, velocity direction $\bar{1}_v$, and kinetic energy density k. Indeed, the major eigenvalue of Π^r_{ik} is $\lambda^{(1)} = p + 2k$ and the corresponding unit eigenvector is the velocity direction $\bar{1}_v$. The other eigenvalues are degenerate ($\lambda^{(2)} = \lambda^{(3)} = p$) in the whole space. It follows that we can only use major tubes. The trajectory of a major tube is everywhere tangent to the velocity direction $\bar{1}_v$ and is a streamline of the velocity field. Furthermore, its cross section is circular, with a diameter proportional to the pressure p. Here, we determine the tube's color by the function

$$color \sim \frac{\lambda^{(1)} - 0.5\left(\lambda^{(2)} + \lambda^{(3)}\right)}{2} = k \qquad \textbf{(4)}$$

which represents the kinetic energy density k. Thus, the trajectory of a major tube encodes the velocity direction, its diameter encodes the pressure, and its color encodes the kinetic energy density.

Figure 4 shows Π^r_{ik} in the flow past a hemisphere cylinder. The direction of the incoming flow is five degrees to the left of the hemisphere axis. You can clearly see the detachment at the end of the cylinder. The pattern of hyperstreamlines indicates that the momentum is transferred from the tip of the body to the end fairly uniformly and with a globally decreasing kinetic energy (as shown by color variations). However, there is a region in the flow where direction, color, and diameter of the first five tubes vary suddenly. These variations indicate correlated changes in velocity direction, kinetic energy density, and pressure, respectively.

Color coding schemes

Usually, color encodes the longitudinal eigenvalue to represent the whole tensor data along the trajectory. In practice, we can modify the color scheme to reveal other aspects of the data. An example is the color coding function of Equation 4, which let us decouple pressure and kinetic energy density when visualizing t e reversible momentum transfers in a flow. For stresses in solids or viscous stresses in fluids, we can use color to discriminate between compressive and tensile directions in a tube's cross section. We do this by coloring the tube at every point according to

$$color \sim \cos(\varphi) \qquad \textbf{(5)}$$

where φ is the angle between two vectors, $\bar{n}$ and $\bar{f}$. $\bar{n}$ is a unit radial vector in the plane of the tube's cross section, and $\bar{f} = \mathbf{U}\bar{n}$ is the force acting on a facet with normal $\bar{n}$. Figure 5 represents the same minor tube as in Figure 2, but we colored it according to Equation 5. Red corresponds to $\varphi = 0$ degrees and indicates that the corresponding directions n are in pure tension. Blue indicates purely compressive directions ($\varphi = 180$ degrees), and green reveals pure shear ($\varphi = 90$ degrees).

When using Equation 5's color function for other tensor data, we lose the meaning of compressive and tensile directions. However, this scheme encodes the sign of the transverse eigenvalues: a principal direction of the elliptical cross section is red if the corresponding eigenvalue is positive and blue if the corresponding eigenvalue is negative.

Figure 5. The minor tube of Figure 2 colored as a function of the normal force. Here we used Color Scale B.

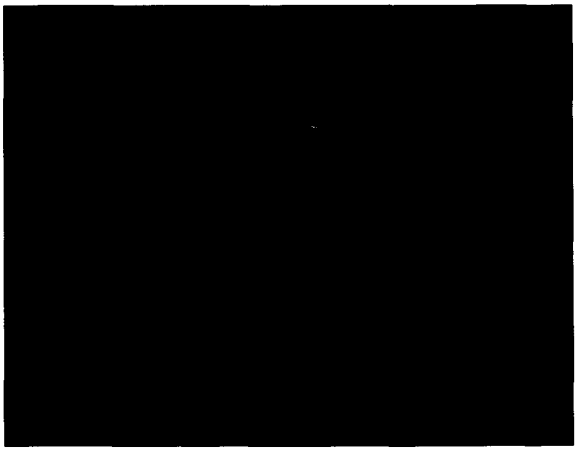

Figure 6. Structural depiction of the stress tensor of Figure 1.

Structural depiction of symmetric tensor fields

Two factors limit the practicality of hyperstreamlines:

1. The resulting display depends on the initial conditions of integration.
2. A large number of hyperstreamlines produces visual clutter.

The same problems arise in 3D scalar and vector field visualization. For example, when visualizing a scalar field with isosurfaces, we get a final image that depends on the isosurfaces we choose. And we can display only a few of these isosurfaces simultaneously. Also, when we use conventional streamlines to visualize a vector field, we get a display dependent on the initial conditions of integration, and too many streamlines clutter the image. With streamlines, we can overcome these problems with algorithms that automatically extract the vector field topology.[6,7] We can think of these algorithms as a way of coding the collective behavior of a large set of vector streamlines. Using an approach analogous to these vector techniques, we can get a structural depiction of tensor data by coding the collective behavior of a large number of hyperstreamlines.

Consider the collection $\{HS^{(i)}\}$ of hyperstreamlines propagating along the eigenvector field $\overline{v}^{(i)}$, as given by Equation 1. Important features exist in both the trajectory and the cross section of these hyperstreamlines. For example, the locus

$$\lambda^{(i)} = 0$$

is the set of the critical points in the trajectory of the hyperstreamlines $\{HS^{(i)}\}$. (At a critical point of a vector field, the magnitude vanishes and the direction of the streamline is locally undefined. Chong, Perry, and Cantwell discuss this more completely.[8]) Further, the surface

$$\lambda^{(j)}\lambda^{(k)} = 0$$

where $\lambda^{(j)}$ and $\lambda^{(k)}$ are the transverse eigenvalues, is the locus of points where the cross section of the hyperstreamlines $\{HS^{(i)}\}$ is singular. That is, the hyperstreamlines' cross section is reduced to a straight line or a point. In general, a surface of constant eccentricity is the locus of points where the cross section of each hyperstreamline in $\{HS^{(i)}\}$ has the same shape, regardless of its orientation and scaling. In particular, the locus

$$\lambda^{(j)} \pm \lambda^{(k)} = 0$$

is the set of points where the cross section degenerates into a circle (zero eccentricity).

Figure 7. (a) Stress tensor and (b) viscous-stress tensor in the flow past a hemisphere cylinder. We used Color Scale A.

Figure 8. Examples of line tensor icons for two different unsymmetric tensor fields: (a) symmetric/antisymmetric decomposition and (b) polar decomposition. We used Color Scale A for tubes and B for ribbons.

In Figure 6, we depict the structure of the stress tensor of Figure 1. The yellow surface is the locus of critical points of the medium eigenvector $\bar{v}^{(2)}$, and the green surface represents the critical points of the major eigenvector $\bar{v}^{(1)}$. On both of these surfaces, the cross section of each minor tube (four of them are shown) reduces to a straight line. On the blue surface, the transverse eigenvalues are opposite to each other, and the cross section is circular. Below the yellow surface, both transverse eigenvalues are positive and every transverse direction in the cross section of the minor tubes is in tension. Above the yellow surface, the medium eigenvalue becomes negative and some transverse directions are in tension while others are compressive. Inside the green surface, however, every transverse direction is in compression.

Stress and viscous-stress tensors in flows

We give another example of structural depiction for the stress tensor σ_{ik} and the viscous-stress tensor σ'_{ik} in fluid flows. As shown in Table 1, these two tensors differ only by an isotropic pressure component. This implies that the unit eigenvectors of both tensor fields are identical. However, the eigenvalues of σ_{ik} are equal to the eigenvalues of σ'_{ik} minus a large pressure component. Table 1 also shows that visualizing σ'_{ik} is equivalent to visualizing the rate-of-strain tensor ε_{ik} in incompressible flows.

In Figure 7a, we show hyperstreamlines of the stress tensor in the flow past a hemisphere cylinder. (The flow is the same as in Figure 4.) The major tubes in front are along the least compressive direction $\bar{v}^{(1)}$. Their trajectory shows how forces propagate from the region in front of the cylinder to the surface of the body. The cross section of the tubes is circular, indicating that the pressure component of the stresses is dominant, as expected. However, the viscous stresses close to the body create a slightly anisotropic cross section. On the yellow surface, the eccentricity of every major tube's cross section equals 10 percent.

The helices are along the medium eigenvector field. They propagate mainly parallel to the cylinder surface and the orientation of their arms indicates a fairly constant direction of the two transverse eigenvectors. The third helix exhibits a more complex behavior, suggesting that the stress tensor is less uniform in the region of contact between the tubes and the body than in other parts of the flow.

Figure 7b shows the viscous-stress tensor σ'_{ik} in the same flow. As expected, the trajectories are similar to those in Figure 7a, but when we removed the large isotropic pressure contribution, we dramatically enhanced the anisotropy of the tube's cross section. The surface corresponds to a constant eccentricity of 90 percent and is crossed twice by each tube.

Unsymmetric tensor fields

We can use hyperstreamlines to visualize symmetric tensor fields whose three eigenvector fields $\bar{v}^{(i)}$ (as given by Equation 1) are real and orthogonal. However, visualizing unsymmetric 3×3 tensor fields $\mathbf{T} = \{T_{ik}\}$ is more difficult because their eigenvectors $\bar{v}^{(i)}$ are generally complex and not orthogonal. A 3D vector field visualization technique, the *stream polygon*,[9] can reveal aspects of vector field gradients. However, the stream polygon does not apply to other kinds of unsymmetric data, and this technique only partially renders the tensor information, even for vector gradients.

We can always decompose unsymmetric tensor data into two components: a symmetric tensor field and a vector field. As before, we visualize the symmetric tensor field with hyperstreamlines. However, to represent the complete (unsymmetric) tensor information, we need to encode the additional vector field along the trajectory. Depending on the physics involved, we can reduce the unsymmetric data in two ways—symmetric/antisymmetric decomposition or polar decomposition.

Symmetric/antisymmetric decomposition

We can decompose the tensor field $\mathbf{T}$ into the sum of symmetric and antisymmetric components according to

$$\mathbf{T} = \frac{\mathbf{T} + \mathbf{T}^t}{2} + \frac{\mathbf{T} - \mathbf{T}^t}{2}$$

where $\mathbf{T}^t$ is the transpose of $\mathbf{T}$. The antisymmetric tensor has only three independent components that form a vector known as the axial vector.[1,10] For instance, the velocity gradient in fluids is the sum of the rate-of-strain tensor ε_{ik} (symmetric) and the rate-of-rotation tensor (antisymmetric) that is half the vorticity vector.

Figure 8a shows a line tensor icon for unsymmetric data based on this decomposition. We integrated a hyperstreamline along

Figure 9. Polar decomposition of unsymmetric data.

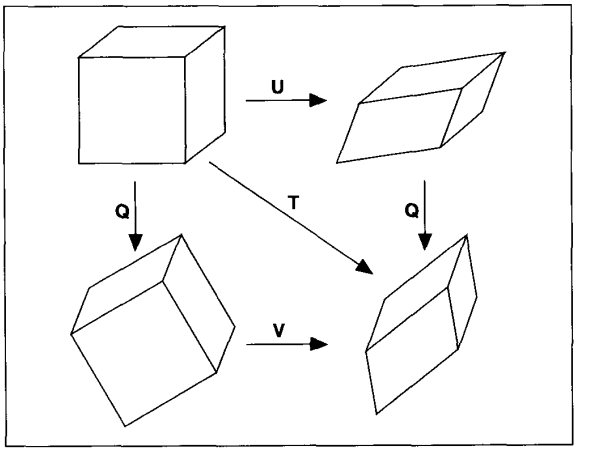

one eigenvector field $\bar{v}^{(i)}$ of the symmetric tensor component. We then color-coded the hyperstreamline according to the longitudinal eigenvalue. Alternatively, we could have applied the color scheme of Equation 5. We added a ribbon outside the tube surface to represent the axial vector. The ribbon position and width encode locally the vector component perpendicular to the trajectory. The color of the ribbon maps the angle between the axial vector and the direction of propagation of the tube according to Color Scale B (red is parallel, green is perpendicular, and blue is antiparallel). In Figure 8a for example, the color shows that the vector field is everywhere close to alignment with the direction of propagation (left to right). It is, however, not exactly aligned, since the ribbon has a finite width.

When visualizing the velocity gradient in fluid flows, we use this icon to show the position of the vorticity with respect to the principal strains. This is an important factor for understanding turbulence.[11]

Polar decomposition

An alternative reduction of the unsymmetric data is *polar decomposition*.[10] Polar decomposition is a generalization to tensors (or matrices in general) of the usual decomposition of a complex number into the product of an amplitude and a phase. Assume, as we did for Figure 9, that the tensor **T** at a given point $\bar{x}$ maps the vertices of a cube from an initial state to a final deformed state. We can decompose this global deformation into more elementary transformations. For example, we can first stretch the cube by a tensor **U** and then rotate the stretched rhomboid by an isometric transformation **Q** to reach the final state. Alternatively, we can first rotate the cube and then stretch it by the tensor **V**.

Mathematically, these are two equivalent ways of decomposing the unsymmetric data into the product of a stretch tensor **U** or **V** (the amplitudes) with an isometric transformation **Q** (the phase):

$$\mathbf{T} = \mathbf{QU} = \mathbf{VQ} \tag{6}$$

where

$$\mathbf{Q} = \mathbf{TU}^{-1}$$

is an orthogonal tensor and both

$$\mathbf{U} = \sqrt{\mathbf{T}^t\mathbf{T}}$$

and

$$\mathbf{V} = \sqrt{\mathbf{T}\mathbf{T}^t}$$

are symmetric positive definite tensors. That is, they are symmetric tensors that have real and positive eigenvalues. We can show[10] that, wherever $\det\mathbf{T} \neq 0$, this decomposition is unique. That is, there is a one-to-one correspondence between the matrix **T** and the set of matrices {**Q**, **U**, and **V**}. We will explain below how we handle points where $\det\mathbf{T} = 0$. From now on, we restrict our discussion to the first decomposition in Equation 6 without loss of generality.

Figure 8b shows a line tensor icon for **T** based on this decomposition. The symmetric tensor **U** is represented by a tube along one of its eigenvectors. In regions where $\det\mathbf{T} > 0$, the isometric transformation **Q** is simply a rotation and is characterized by an angle θ ($0 \le \theta \le \pi$) and a unit axis of rotation $\bar{u}$. Thus, we can represent **Q** by the vector

$$\bar{r}^{(1)} = \theta\ \bar{u}$$

However, a rotation of angle θ about the axis $\bar{u}$ is physically identical to a rotation of angle $2\pi - \theta$ about the axis $-\bar{u}$. Thus, **Q** is also equivalent to the vector

$$\bar{r}^{(2)} = (2\pi - \theta)(-\bar{u})$$

To visualize **Q**, we added two ribbons that represent the vectors $\bar{r}^{(1)}$ and $\bar{r}^{(2)}$. Note that in regions where $\det\mathbf{T} < 0$, the transformation **Q** involves an additional inversion in the direction of the rotation axis. A row of white pearls across the ribbons marks the onset of the inversion during the propagation. A row of black pearls indicates its cancellation.

Singular points

In some points of the trajectory, the vectors $\bar{r}^{(1)}$ and $\bar{r}^{(2)}$ might not be defined. We then simply interpolate them between adjacent points to avoid discontinuities in the ribbons. These singular points occur

1. at the pearls where $\det\mathbf{U} = |\det\mathbf{T}| = 0$ (**U** is defined but not invertible and **Q** cannot be computed) and
2. where **Q** reduces to plus or minus the identity matrix (the rotation axis $\bar{u}$ is undefined and **T** is locally symmetric with all eigenvalues having the same sign).

Thus, we assume that these singularities are isolated points along the trajectories. This approach fails only if there is an entire subvolume where Condition 1 occurs. Indeed, in subvolumes where Condition 2 occurs, the data is symmetric, and we can use hyperstreamlines without additional ribbons.

Conclusions

We extracted and rendered the wealth of information contained in second-order tensor data as hyperstreamlines. By continuously representing both the amplitude and the directional information typical of tensor data, hyperstreamlines reveal much of the physics involved in complicated processes that are otherwise only partially visualized in terms of vector or scalar functions. Hyperstreamlines are the simplest continuous tensor structures that we can extract from symmetric or unsymmetric tensor fields. Coding hyperstreamlines' collective behavior is a first step in obtaining a structural depiction of tensor fields, analogous to extracting vector field topology.

In future work, we must obtain more advanced structural depictions. To do this, we might enhance the techniques presented in this article by focusing on specific physical properties of particular tensor fields. ❑

Acknowledgments

We thank Yuval Levy for providing us with the fluid flow data sets and Paul Ning for his initial implementation of the marching cubes algorithm on which we based our isosurface extraction algorithm. This work is supported by NASA under contracts NAG 2-701 and NCA 2-579, and by the National Science Foundation under grant ECS8815815.

References

1. A.I. Borisenko and I.E. Tarapov, *Vector and Tensor Analysis with Applications*, Dover Publications, New York, 1979.
2. T. Delmarcelle and L. Hesselink, "Visualization of Second-Order Tensor Fields and Matrix Data," *Proc. IEEE Visualization 92*, CS Press, Los Alamitos, Calif., 1992, pp. 316-323.
3. R.B. Haber, "Visualization Techniques for Engineering Mechanics," *Computing Systems in Engineering*, Vol. 1, No. 1, Jan. 1990, pp. 37-50.
4. R.B. Haber and D.A. McNabb, "Visualization Idioms: A Conceptual Model for Scientific Visualization Systems," in *Visualization in Scientific Computing*, G.M. Nielson and B. Shriver, eds., CS Press, Los Alamitos, Calif., 1990, pp. 74-93.
5. R. Dickinson, "A Unified Approach to the Design of Visualization Software for the Analysis of Field Problems," *3D Visualization and Display Technologies* (Proc. SPIE), Vol. 1083, Jan. 1989, SPIE (International Society for Optical Engineering), Bellingham, Wash., pp. 173-180.
6. J. Helman and L. Hesselink, "Visualizing Vector Field Topology in Fluid Flows," *IEEE CG&A*, Vol. 11, No. 3, May 1991, pp. 36-46.
7. A. Globus, C. Levit, and T. Lasinski, "A Tool for Visualizing the Topology of 3D Vector Fields," *Proc. IEEE Visualization 91*, CS Press, Los Alamitos, Calif., 1991, pp. 33-40.
8. M.S. Chong, A.E. Perry, and B.J. Cantwell, "A General Classification of Three-Dimensional Flow Fields," *Physics of Fluids A*, Vol. 2, No. 5, May 1990, pp. 36-46.
9. W.J. Schroeder, C.R. Volpe, and W.E. Lorensen, "The Stream Polygon: A Technique for 3D Vector Field Visualization," *Proc. IEEE Visualization 91*, CS Press, Los Alamitos, Calif., 1991, pp. 126-132.
10. D.C. Leigh, *Nonlinear Continuum Mechanics*, McGraw-Hill, New York, 1968.
11. W.T. Ashurst et al., "Alignment of Vorticity and Scalar Gradient with Strain Rate in Simulated Navier-Stokes Turbulence," *Physics of Fluids*, Vol. 30, No. 8, Aug. 1987, pp. 2,343-2,353.

Thierry Delmarcelle is a research assistant in the Fourier Optics and Optical Diagnostics Laboratory at Stanford, where he is completing work on a PhD in applied physics. His dissertation is on the representation of tensor fields, and his other research interests include multivariate data visualization, flow visualization, computer graphics, and color perception.

Delmarcelle received a degree in physics engineering from the Faculté des Sciences Appliquées of the Université Libre de Bruxelles (Brussels, Belgium) in 1988 and a MS in applied physics from Stanford in 1991.

Delmarcelle can be reached at the Department of Applied Physics, Stanford University, Stanford, CA 94305-4090.

Lambertus Hesselink is a professor in the electrical engineering and aeronautics and astronautics departments at Stanford University. His research interests include nonlinear optics, optical phase conjugation, optical signal processing, optical computing, optical diagnostics, and 3D image processing.

Hesselink received a BS in applied mechanics and a separate BS in applied physics from the Twente Institute of Technology in the Netherlands. He received his MS and PhD from the California Institute of Technology. He is a fellow of the Optical Society of America.

Hesselink can be reached at the Department of Aeronautics and Astronautics, Durand Building, Room 353, Stanford University, Stanford, CA 94305-4035.